

# **Tuning electrochemical and transport processes to achieve extreme performance and efficiency in solid oxide cells**

Beom-Kyeong Park, Roberto Scipioni, Qian Zhang, Dalton Cox, Peter W. Voorhees, and  
Scott A. Barnett \*

*Department of Materials Science and Engineering, Northwestern University, Evanston, Illinois  
60208, USA*

**\* Corresponding author**

E-mail: [s-barnett@northwestern.edu](mailto:s-barnett@northwestern.edu)

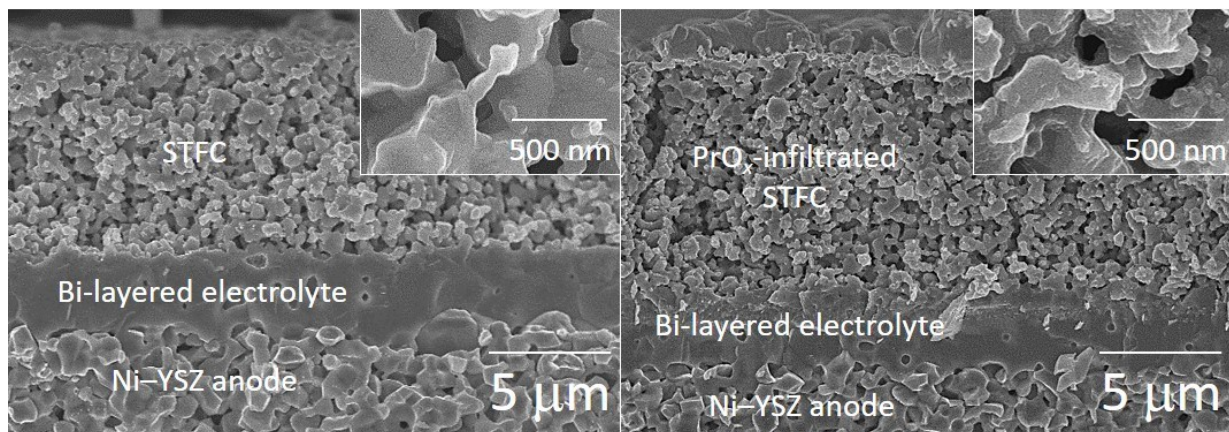


**Fig. S1** Post-test SEM images of the Baseline and PrO<sub>x</sub> cells.

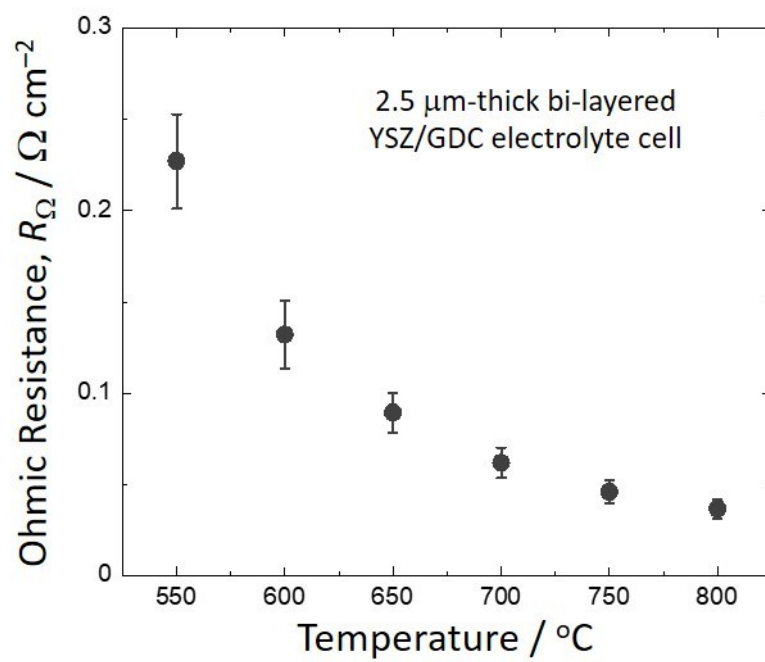


**Fig. S2** Ohmic resistances ( $R_{\Omega}$ ) as a function of temperature for  $\sim 2.5 \mu\text{m}$ -thick bi-layered GDC/YSZ electrolyte cells produced in this work.

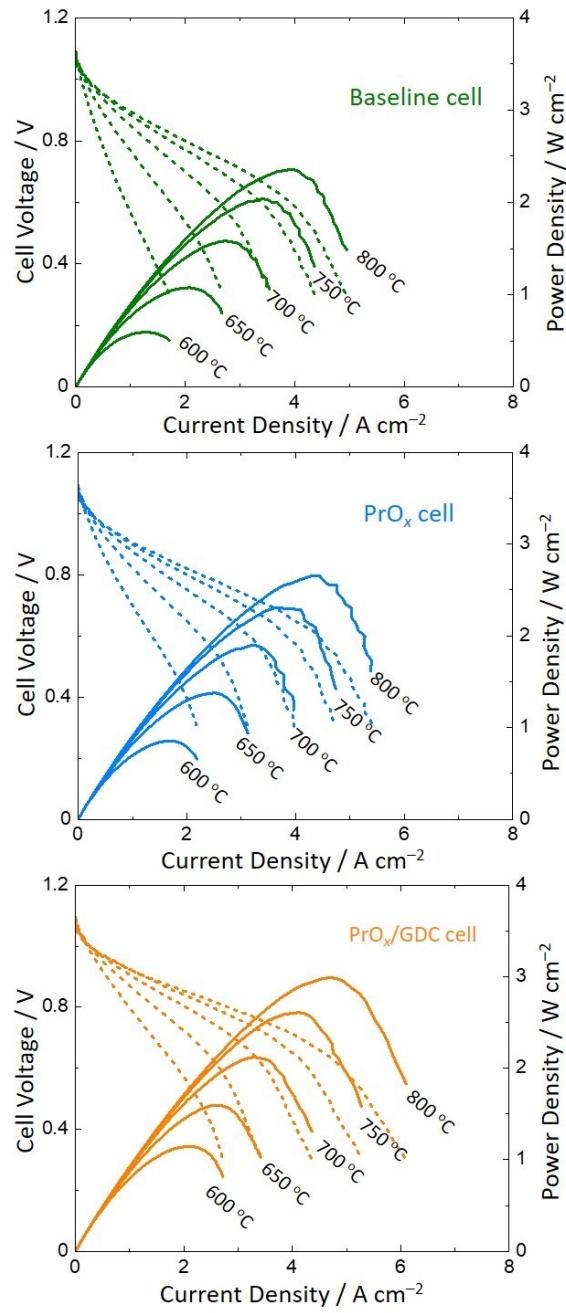


**Fig. S3**  $j$ - $V$  curves and power densities of the Baseline, PrO<sub>x</sub>, and PrO<sub>x</sub>/GDC cells at 600–800 °C in 97 vol.% H<sub>2</sub>–3 vol.% H<sub>2</sub>O and air.

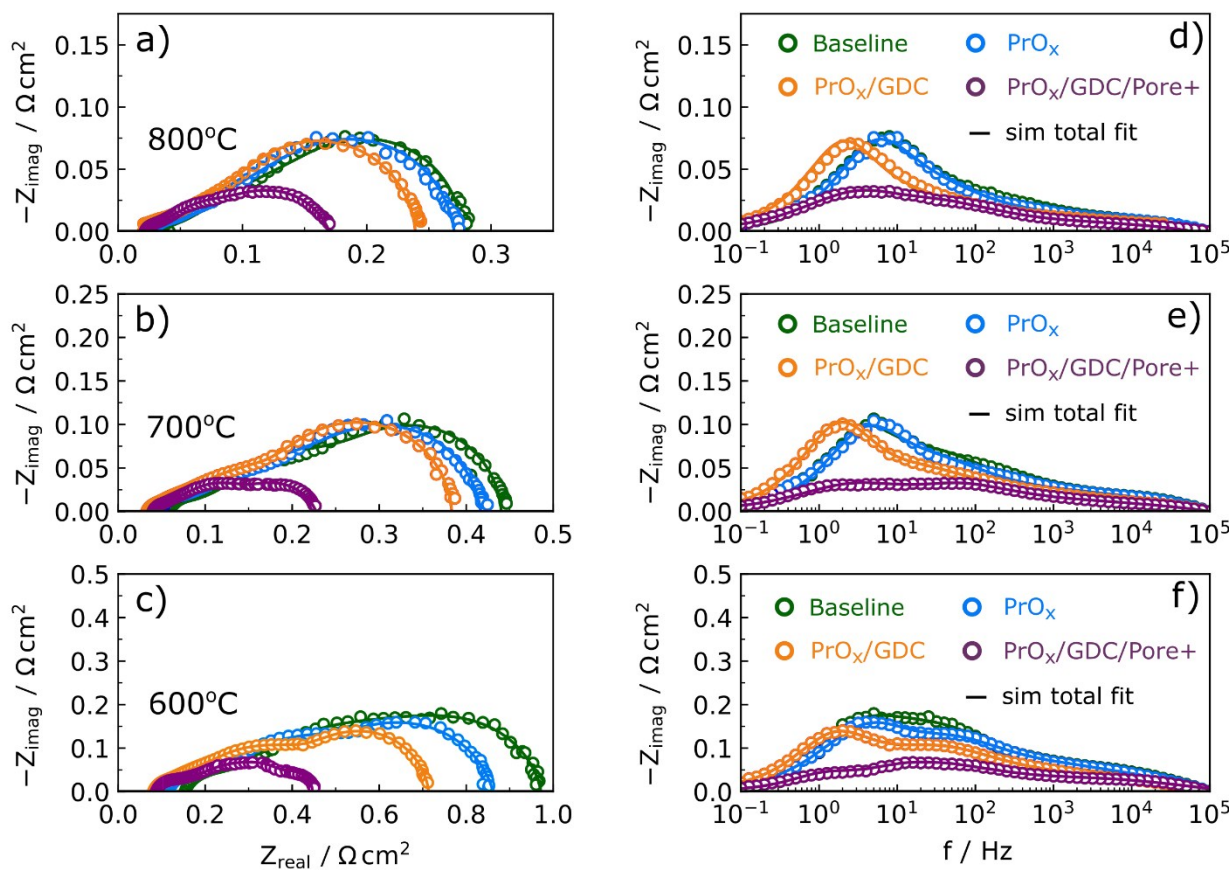


**Fig. S4** Comparison of impedance spectra of the Baseline,  $\text{PrO}_x$ ,  $\text{PrO}_x/\text{GDC}$ , and  $\text{PrO}_x/\text{GDC}/\text{Pore+}$  cells at 600, 700 and 800 °C in 97 vol.%  $\text{H}_2$ -3 vol.%  $\text{H}_2\text{O}$  and air. Best fits to the data, using the model described in the text, are shown as solid lines.

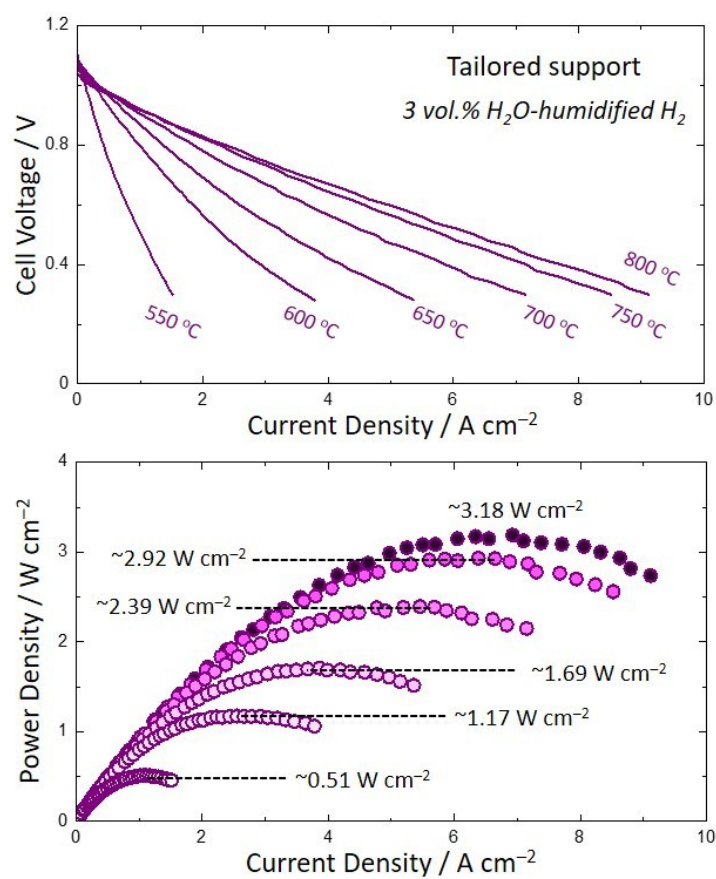


**Fig. S5**  $j$ - $V$  curves and power densities of the PrO<sub>x</sub>/GDC/Pore+ cell at 550–800 °C in 97 vol.% H<sub>2</sub>–3 vol.% H<sub>2</sub>O and air.

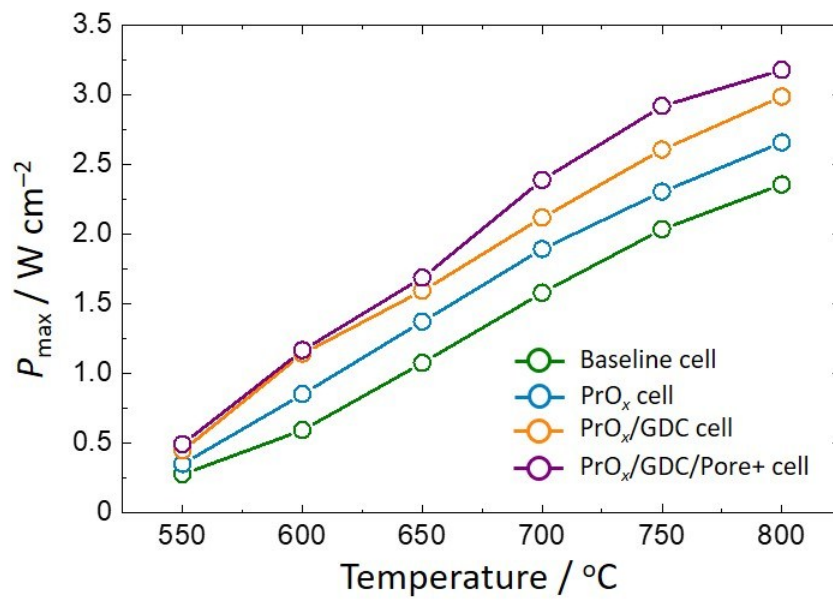


**Fig. S6** Maximum power densities ( $P_{\max}$ ) as a function of temperature for the Baseline,  $\text{PrO}_x$ ,  $\text{PrO}_x/\text{GDC}$ , and  $\text{PrO}_x/\text{GDC}/\text{Pore+}$  cells.

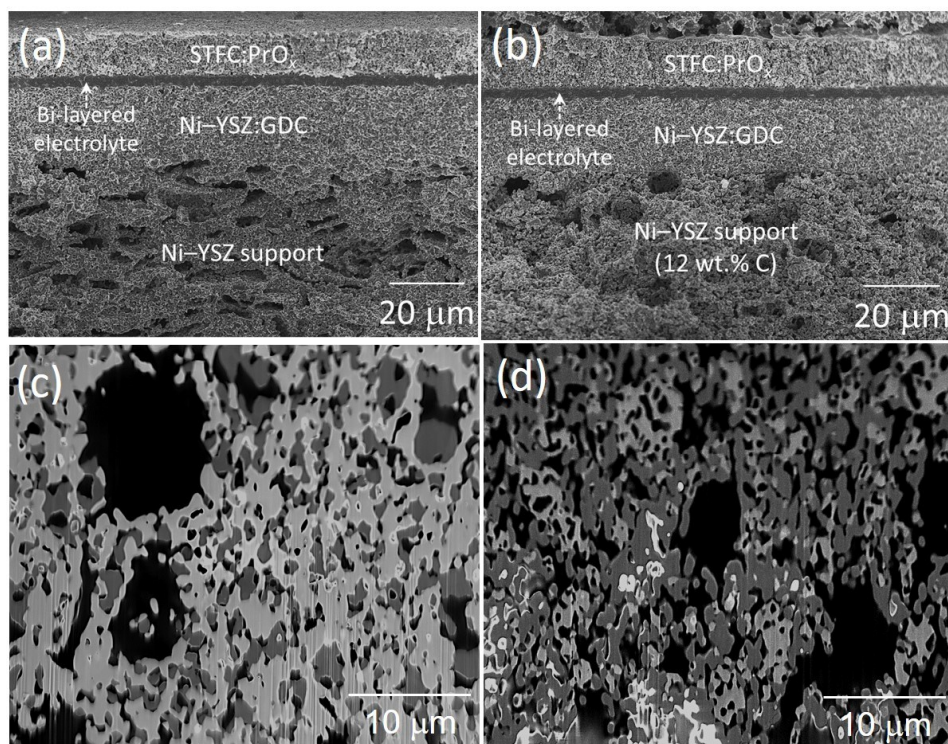


**Fig. S7** Fractured surface SEM images of the (a) PrO<sub>x</sub>/GDC and (b) PrO<sub>x</sub>/GDC/Pore+ cells. Polished cross-sectional SEM images of the anode support layer (ASL) of the (c) PrO<sub>x</sub>/GDC and (d) PrO<sub>x</sub>/GDC/Pore+ cells.

The sample was polished up to a 1 μm polishing solution on the top and imaging sides, then a high current Ga beam was used to rough cut the surface, leaving behind the curtaining. A low current beam was then applied as a cleaning cut to remove the large curtaining. While the black color indicates the pore, the bright and dark gray colors indicate the Ni and YSZ, respectively.

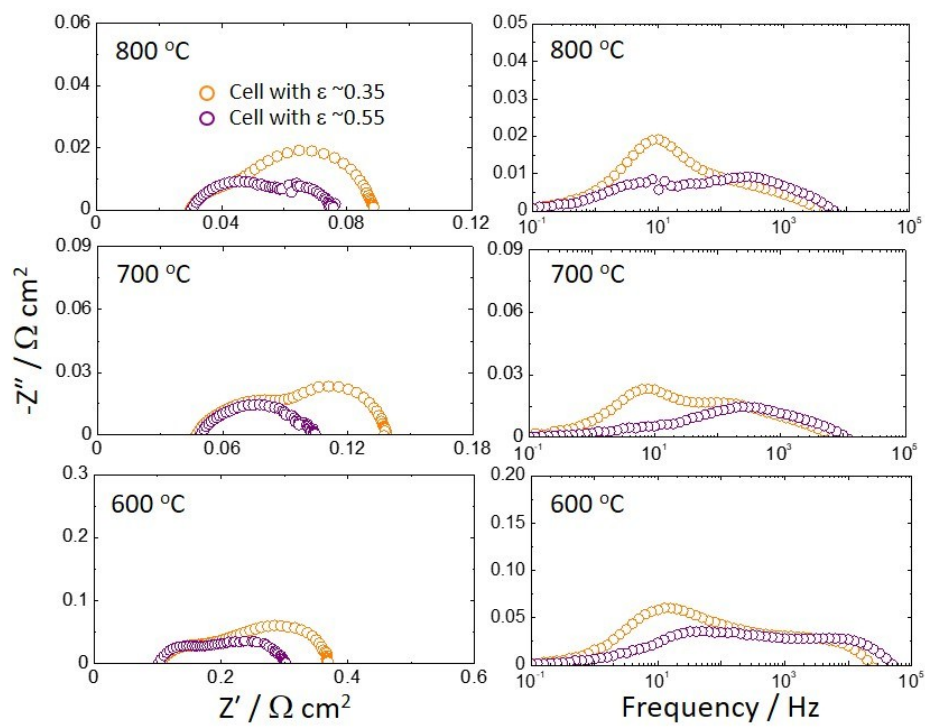


**Fig. S8** Comparison of impedance spectra for the  $\text{PrO}_x/\text{GDC}$  and  $\text{PrO}_x/\text{GDC}/\text{Pore}+$  cells measured at 600, 700, and 800 °C in 50 vol.%  $\text{H}_2$ –50 vol.%  $\text{H}_2\text{O}$  and air.

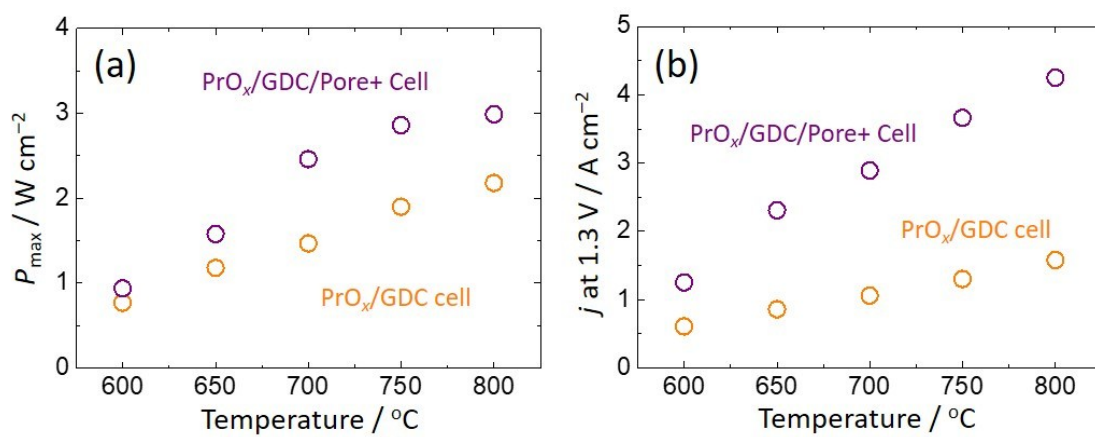


**Fig. S9** Comparison of (a) maximum power densities ( $P_{\max}$ ) and (b) current densities ( $j$ ) at 1.3 V in fuel cell and electrolysis modes, respectively, for the PrO<sub>x</sub>/GDC and PrO<sub>x</sub>/GDC/Pore+ cells.

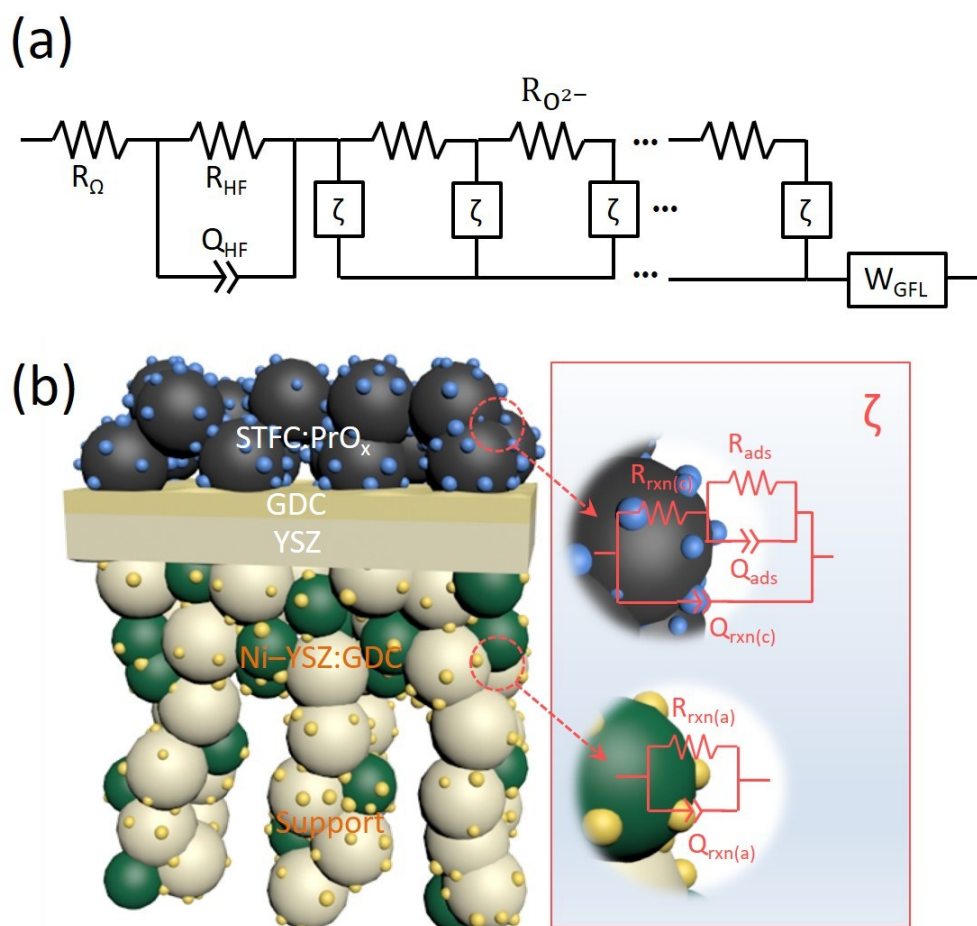


**Fig. S10** (a) Equivalent circuit model (ECM) used to fit the EIS data of the  $\text{PrO}_x/\text{GDC}$  and  $\text{PrO}_x/\text{GDC}/\text{Pore}+$  cells. The ECM is composed of a transmission line model (TLM) which includes an interfacial element  $\zeta$ , better described in the schematic representation in (b).

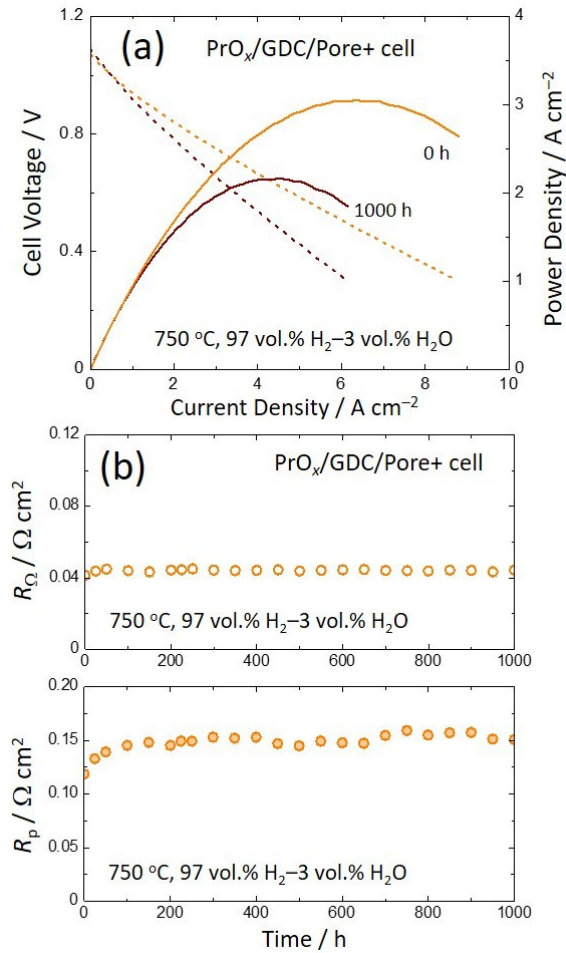


**Fig. S11** (a)  $j$ - $V$  curves and power densities of the PrO<sub>x</sub>/GDC/Pore+ cell before and after the life test performed at 750 °C in 97 vol.% H<sub>2</sub>-3 vol.% H<sub>2</sub>O and air. (b) Evolution of the ohmic ( $R_{\Omega}$ ) and polarization ( $R_p$ ) resistances of the PrO<sub>x</sub>/GDC/Pore+ cell during the life test of 1000 h performed at 750 °C in 97 vol.% H<sub>2</sub>-3 vol.% H<sub>2</sub>O and air.

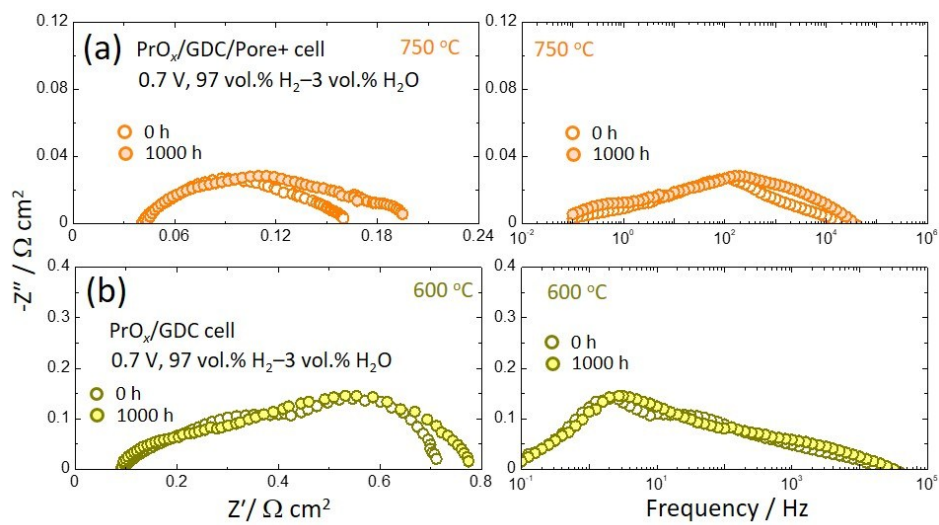


**Fig. S12** Comparison of the impedance spectra in Nyquist and Bode plots for the cells in before and after the life tests performed at (a)  $750\text{ }^\circ\text{C}$  and (b)  $600\text{ }^\circ\text{C}$  in  $97\text{ vol.}\% \text{H}_2\text{-}3\text{ vol.}\% \text{H}_2\text{O}$  and air.

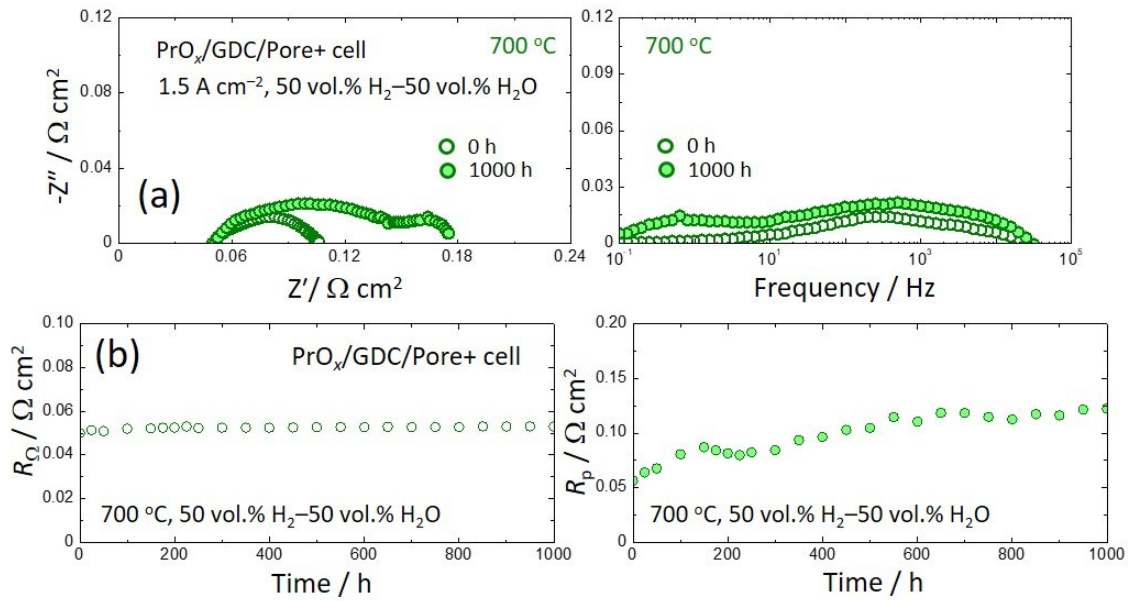


**Fig. S13** (a) Comparison of the impedance spectra in Nyquist and Bode plots for the cell before and after the life test in Fig. 7b. (b) Evolution of the ohmic ( $R_\Omega$ ) and polarization ( $R_p$ ) resistances of the  $\text{PrO}_x/\text{GDC}/\text{Pore+}$  cell during the life test of 1000 h performed at 700 °C in 50 vol.%  $\text{H}_2$ –50 vol.%  $\text{H}_2\text{O}$  and air.

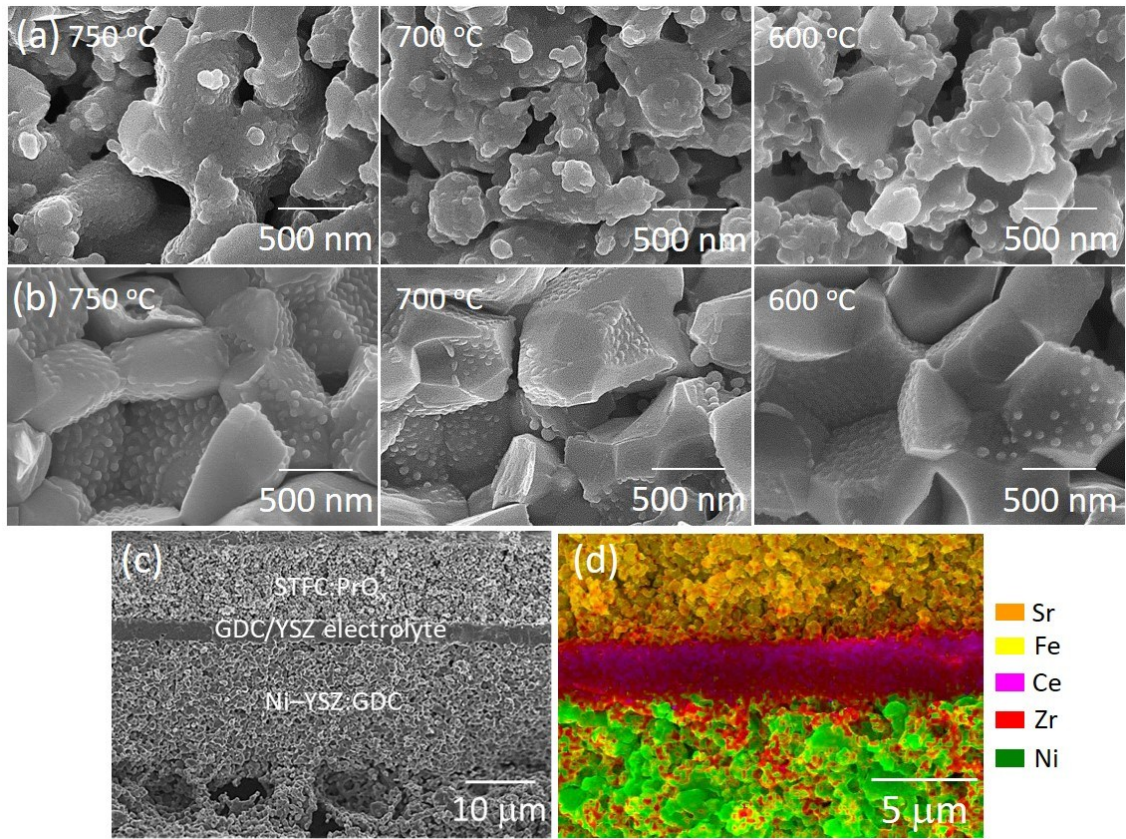


**Fig. S14** Post-test SEM images for the (a) STFC:PrO<sub>x</sub> and (b) Ni-YSZ:GDC electrodes for the PrO<sub>x</sub>/GDC and PrO<sub>x</sub>/GDC/Pore+ cells after the life tests in Figs. 7a and b. (c) Post-test SEM images of the PrO<sub>x</sub>/GDC/Pore+ cell after the life test in Fig. 7b. (d) The EDS elemental maps for Sr, Fe, Ce, Zr, and Ni elements from a fractured surface of the PrO<sub>x</sub>/GDC/Pore+ cell in (c).

Figs. S14a and b show the electrode microstructures of oxygen and fuel electrodes, respectively, for the tested cells in Fig. 7. Compared to the morphologies at the beginning stage (Figs. 1c and d), it could be shown that the particle coarsening for PrO<sub>x</sub> and GDC occurred rather at higher temperatures, which could explain the reason why  $R_p$  increased during the life tests at 700 and 750 °C. The EDS chemical maps in Figs. 1b and S14d show that the elements

were restricted within their respective layers, suggesting the excellent chemical compatibility among the cell components during the life tests. Along with the robust interface for tested cell in Fig. S14c, the lack of damage at interfaces (GDC/YSZ and electrode/electrolyte) is consistent with the stable  $R_{\Omega}$  during the life test in Fig. S13b. Note that GDC infiltration in particular has been shown to mitigate degradation Ni-YSZ/YSZ region during electrolysis<sup>1</sup>. In summary, these structural/chemical analyses demonstrate the high integrity of cells under various SOC operating conditions.

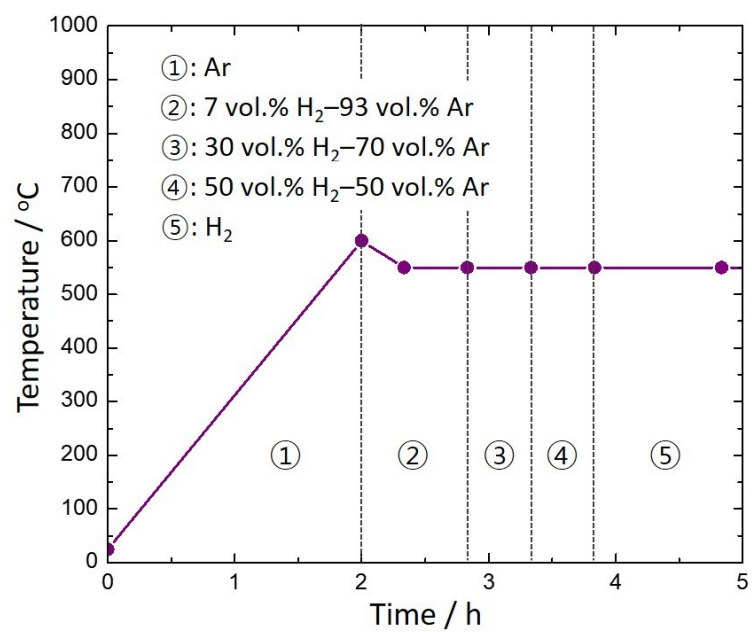


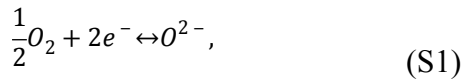
**Fig. S15** The SOC activation procedure for the  $\sim 2.5$   $\mu\text{m}$ -thick bi-layered GDC/YSZ electrolyte cells.

**Table S1.** The electrode materials and support porosity of cells produced in this work.

<i>Cell Name</i>	<i>Baseline</i>	<i>PrO<sub>x</sub></i>	<i>PrO<sub>x</sub>/GDC</i>	<i>PrO<sub>x</sub>/GDC/Pore+</i>
<i>Oxygen electrode</i>	STFC	STFC:PrO <sub>x</sub>	STFC:PrO <sub>x</sub>	STFC:PrO <sub>x</sub>
<i>Fuel electrode</i>	Ni-YSZ	Ni-YSZ	Ni-YSZ:GDC	Ni-YSZ:GDC
<i>Support</i>	Low porosity	Low porosity	Low porosity	High porosity

This section provides some background on the model used to get the oxygen partial pressure distribution in the electrolyte.

The chemical reactions within the electrolyte, during the electrolysis operation, can be described:



For the mixed (electronic and ionic) conductor, the flux ( $j_x$ ) of various species, such as electron (e), hole (h), and oxygen ion ( $O^{2-}$ ), are determined by the following equation:

$$j_x = -\frac{D_x}{RT} C_x \nabla \bar{\mu}_x = -D_x \nabla C_x - \frac{z_x F}{RT} D_x C_x \nabla \phi, \quad x = e, h, O^{2-} \quad (S3)$$

where  $D$ ,  $C$ ,  $\bar{\mu}$ ,  $z$ , and  $\phi$  are diffusivity, concentration, electrochemical potential, charge valance of corresponding species, and Galvani potential, respectively, and  $R$ ,  $T$ , and  $F$  have their usual meanings. At steady state, total current density ( $j$ ) is calculated:

$$j = F(j_h - j_e - 2j_{O^{2-}}) \quad (S4)$$

Then, the mathematical model is obtained by combining the above equations (eqn (S3) and (S4)) with local equilibrium of reactions (eqn (S1) and (S2)) and charges neutrality. Here, the oxygen partial pressure ( $P_{O_2}$ ) can be calculated using the definition of electrical potential ( $E$ ), which is chemical potential of electron in volt, the local equilibrium conditions in reaction (4), and  $C_e$  derived *via* our model, as below:

$$E = E^0 - \frac{RT}{F} \ln \left( \frac{C_e}{C_e^0} \right) = E^0 + \frac{RT}{4F} \ln \left( \frac{P_{O_2}}{P_{O_2}^0} \right), \quad (S5)$$

where the terms with superscript ‘0’ in eqn (S5) are the corresponding quantities under standard state. The boundary conditions for the calculation are the oxygen-electrode and fuel-electrode overpotentials, which are calculated using eqn (S6) based on measured polarization resistance values for the oxygen electrode  $R_{p,O}(j=0)$  and fuel electrode  $R_{p,H}(j=0)$ . The values were derived the data reported in literature<sup>2-4</sup>, as discussed in this supplement material. All the parameters in the numerical simulation are taken the same as that we obtained in the experimental measurement.

$$\eta = \frac{2RT}{zF} \sinh^{-1} \left( \frac{j}{2j_0} \right); j_0 = \frac{RT}{zFR_p(j=0)}, \quad (S6)$$

This section provides some background on a stereological analysis used to get the porosity ( $\varepsilon$ ) and tortuosity ( $\tau$ ) of pristine and tailored supports.

2D stereological analyses of the Ni–YSZ support microstructures were performed to obtain specific surface area and porosity. Polished epoxy-infiltrated samples were milled and imaged at 8000 $\times$  magnification using an FEI Helios FIB-SEM. Images of the electrode were taken in a manner to avoid biasing the results: there was no overlap in images in the x–y plane and milling depth in the z direction was greater than the largest particle size to ensure independence of the sampled areas.

Using in-house MATLAB code, the SEM images (Fig. S7) were binaried into solid and pore phases and the total length of interface of the two phases in each 2D image was calculated. Porosity and specific surface area were estimated using the equations:

$$\varepsilon = \varepsilon_A \quad (\text{S7})$$

$$a = (4L_A)/\pi \quad (\text{S8})$$

Where  $\varepsilon_A$  is the 2D porosity of the image and  $L_A$  is the interface length divided by the area of the image<sup>5</sup>. Values obtained for each image were averaged within the composition dataset. To verify the method, the stereological calculations were performed on previously obtained full 3D reconstruction datasets. It was found that 10 independent images (no particle overlap between images) of the 300 image datasets was sufficient to ensure that 3D porosity and surface area values fell within the error of stereological measurement.

## Reference

- 1 Ovtar, S. *et al.* Boosting the performance and durability of Ni/YSZ cathode for hydrogen production at high current densities via decoration with nano-sized electrocatalysts. *Nanoscale* **11**, 4394–4406 (2019).
- 2 Park, B.-K., Zhang, Q., Voorhees, P. W. & Barnett, S. A. Conditions for stable operation of solid oxide electrolysis cells: oxygen electrode effects. *Energy Environmen. Sci.* **12**, 3053–3062 (2019).
- 3 Park, B.-K., Scipioni, R., Cox, D. & Barnett, S. A. Enhancement of Ni–(Y<sub>2</sub>O<sub>3</sub>)<sub>0.08</sub>(ZrO<sub>2</sub>)<sub>0.92</sub> fuel electrode performance by infiltration of Ce<sub>0.8</sub>Gd<sub>0.2</sub>O<sub>2–δ</sub> nanoparticles. *J. Mater. Chem. A. accepted* (2020).
- 4 Lu, M. Y. *et al.* Mechanisms of PrO<sub>x</sub> performance enhancement of oxygen electrodes for low and intermediate temperature solid oxide fuel cells. *Mater. Today Energy*, 100362 (2019).
- 5 Cruz-Orive, L. M. Unbiased Stereology: Three-Dimensional Measurement in Microscopy. *J Anat* **194**, 153–157 (1999).